

Atomistic Multiscale Modeling of Colloidal Plasmonic Nanoparticles

Luca Nicoli,[†] Sveva Sodomaco,[†] Piero Lafiosca,[†] Tommaso Giovannini,^{*,‡} and Chiara Cappelli^{*,†}

[†]*Scuola Normale Superiore, Piazza dei Cavalieri 7, 56126 Pisa, Italy.*

[‡]*Department of Physics, University of Rome Tor Vergata, Via della Ricerca Scientifica 1, 00133, Rome, Italy*

E-mail: tommaso.giovannini@uniroma2.it; chiara.cappelli@sns.it

Abstract

A novel fully atomistic multiscale classical approach to model the optical response of solvated real-size plasmonic nanoparticles (NPs) is presented. The model is based on the coupling of the Frequency Dependent Fluctuating Charges and Fluctuating Dipoles ($\omega\text{FQF}\mu$), specifically designed to describe plasmonic substrates, and the polarizable Fluctuating Charges (FQ) classical force field to model the solvating environment. The resulting $\omega\text{FQF}\mu/\text{FQ}$ approach accounts for the interactions between the radiation and the NP, as well as with the surrounding solvent molecules, by incorporating mutual interactions between the plasmonic substrate and solvent. $\omega\text{FQF}\mu/\text{FQ}$ is validated against reference TD-DFTB/FQ calculations, demonstrating remarkable accuracy, particularly in reproducing plasmon resonance frequency shifts for structures below the quantum-size limit. The flexibility and reliability of the approach are also demonstrated by simulating the optical response of homogeneous and bimetallic NPs dissolved in pure solvents and solvent mixtures.

1 Introduction

In the past decades, colloidal nanoparticles (NPs), i.e. NPs dissolved in solution, have gained significant interest due to their applications in many technological contexts, such as sensing,¹ biomedical applications,² optoelectronics,³ and energy conversion.⁴ By choosing different precursors, reducing agents, solvents, and capping agents, nanostructured materials can be synthesized with a fine control of shape and size.⁵ Size, shape, chemical composition, and the solvent can indeed affect the plasmon resonance frequency (PRF), i.e. the maximum of the NP absorption spectrum.⁶ Such a feature is the basis of a particular class of sensors, which exploit the shift of the PRF upon change of the local refractive index (RI) of the solvent in which the plasmonic NPs are dissolved. Such devices have been widely employed in biosensing,^{7,8} where maximizing the induced PRF shift as a function of RI is crucial to enhance sensitivity.^{1,9}

Rationalizing solvent effects on the PRF of colloidal NPs is particularly challenging from a theoretical point of view. In fact, the optical properties of colloidal NPs result from the interplay of complex phenomena originating under the action of the external electric field, such as the appearance of a localized surface plasmon (LSP) excitation and the polarization of the solvent electron cloud. Solvent effects on PRFs result from a delicate balance between NP-solvent electrostatic (and polarization) interactions, charge-transfer effects, and the possible alteration of the plasmon decaying channels.¹⁰

In principle, a proper description of all possible NP-solvent effects would require an *ab initio* treatment of the whole system. However, first principle approaches become rapidly unfeasible due to their unfavorable scaling as a function of the system's size, thus hindering the simulation of realistic systems. For these reasons, commonly exploited theoretical approaches to simulate plasmonic colloidal NPs are rooted in classical physics,^{11–15} generally making use of the classical Mie theory,¹¹ the Boundary Element Method (BEM),¹² the Discrete Dipole Approximation (DDA),¹³ and the Finite Difference Time Domain (FDTD).¹⁴ However, all these approaches are based on approximated descriptions of both the NP and the solvent, which is generally modeled as a continuum dielectric characterized by its specific permittivity ϵ . In addition, such approaches do not retain the atomistic nature of the system.

In this paper, we propose a novel multiscale method where both the plasmonic NP and the solvent are treated at full atomistic level. In particular, we employ the fully atomistic electromagnetic model called Frequency Dependent Fluctuating Charges Fluctuating Dipoles (ω FQF μ)¹⁶ to describe the optical response

of plasmonic NPs. Such a model is remarkably versatile and can be applied to NPs of any shape¹⁶ and chemical composition,¹⁷ even at the quantum size limit (< 5 nm).¹⁶ The solvent is modeled employing the polarizable Fluctuating Charges (FQ) force field,^{18–20} which is specifically designed to model the polarization of the electron cloud of molecular systems. For this reason, it has been widely exploited in the context of computational spectroscopy of solvated systems.^{21–24}

The two approaches, ω FQF μ and FQ, are coupled in a multiscale fashion so that the resulting ω FQF μ /FQ model accounts for the mutual electrostatic interaction between the solvent and the plasmonic NP, allowing for the modeling of the optical properties of generic colloidal plasmonic NPs. ω FQF μ /FQ is also coupled to classical molecular dynamics (MD) simulations, which are exploited to sample the NP-solvent phase space. Therefore, differently from previous methods,^{11,11–14} the dynamical aspects of the solvation phenomenon, which are crucial to properly model solvent effects on spectroscopy, are taken into account.^{21,23,25}

Note that, if solvent molecules are not adsorbed on the surface of the NP, the main solvent effect on plasmonic properties is the local RI variation of the medium surrounding the nanomaterial. This leads to a modification of the local optical field, generally causing a PRF redshift.^{10,26} Such effect is harnessed in many colorimetric-sensors for the detection of specific biomolecular analytes.^{7,8,11,27–34} In this work, we model the physical processes that lead to plasmon shift upon change of the local RI of the embedding medium.

The paper is organized as follows: first, the novel ω FQF μ /FQ approach is presented after the theoretical foundations of ω FQF μ and FQ methods are recalled. Then, the computational protocol is presented and ω FQF μ /FQ is validated in comparison with reference Time-Dependent Density Functional Tight Binding/Fluctuating Charges (TD-DFTB/FQ³⁵) results. The versatility and robustness of the approach are demonstrated by studying real-size homogeneous and bimetallic NPs dissolved in pure solvent or solvent mixtures. A summary and the main conclusions of the work end the manuscript.

2 Theory

In this section, ω FQF μ and FQ are briefly recalled and the ω FQF μ /FQ approach for modeling the optical properties of colloidal plasmonic NPs is presented (see Fig. 1).

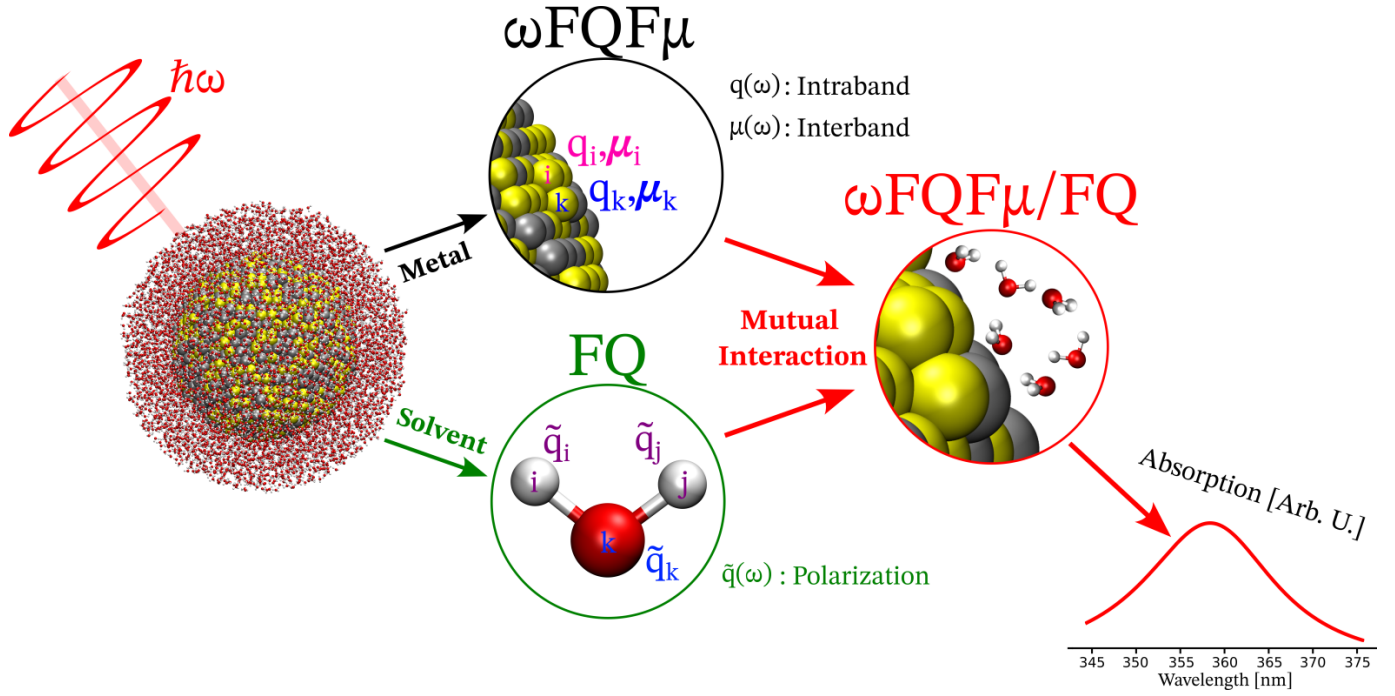


Figure 1: Pictorial view of the multiscale scheme employed to develop $\omega\text{FQF}\mu/\text{FQ}$.

2.1 Plasmonic nanoparticle: the atomistic-electromagnetic $\omega\text{FQF}\mu$ model

$\omega\text{FQF}\mu$ models the plasmonic NP atomistically. Each atom is endowed with a set of complex frequency-dependent atom-centered charges $\mathbf{q}(\omega)$ (ωFQs), and dipoles $\boldsymbol{\mu}(\omega)$ ($\omega\text{F}\mu\text{s}$) (see Fig. 1), accounting for intraband and interband mechanisms, respectively. Charges are obtained by solving the following equation of motion, obtained by modulating a Drude-like conduction mechanics with quantum tunneling:^{36,37}

$$-i\omega q_i(\omega) = \sum_j \left(\frac{A_j n_j (1 - f_{ji}(l_{ij}))}{1/\tau_j - i\omega} + \frac{A_i n_i (1 - f_{ij}(l_{ij}))}{1/\tau_i - i\omega} \right) \frac{\phi_i(\omega) - \phi_j(\omega)}{l_{ij}} \quad (1)$$

In eq.1 A_i , n_i , and τ_i are the atomic effective area, the electron density, and the relaxation time associated with the intraband scattering events of the i -th atom, respectively. Quantum tunneling effects are expressed in terms of a Fermi-like damping function $f_{ij}(l_{ij})$, which exponentially damps the charge exchange between the atoms (l_{ij} is the distance between i -th and j -th atoms). $\phi_i(\omega)$ is the chemical potential of i -th atom, which reads:

$$\phi_i(\omega) = V_i^q(\omega) + V_i^\mu(\omega) + V_i^{\text{ext}}(\omega) \quad (2)$$

where V_i^{ext} is the electric potential associated with the optical radiation, whereas V_i^q and V_i^μ are the electric potentials induced by charges and dipoles on the i -th atomic site (see Ref. 16 for more details).

The plasmonic properties of alkali metals and graphene in the Pauli-blocking regime are correctly described by ω FQs which properly models intraband mechanisms.^{36–38} However, when the interband absorption energy threshold is comparable to the plasmon resonance frequency (PRF), such as in noble metal nanoparticles, interband transitions become relevant to the decaying mechanism.³⁹ To model this process, an additional complex frequency-dependent dipole $\boldsymbol{\mu}(\boldsymbol{\omega})$ is assigned to each atom:

$$\boldsymbol{\mu}_i(\boldsymbol{\omega}) = \alpha_i^{\text{IB}}(\boldsymbol{\omega}) \mathbf{E}_i^{\text{tot}}(\boldsymbol{\omega}) \quad (3)$$

$$= \alpha_i^{\text{IB}}(\boldsymbol{\omega}) [\mathbf{E}_i^q(\boldsymbol{\omega}) + \mathbf{E}_i^\mu(\boldsymbol{\omega}) + \mathbf{E}_i^{\text{ext}}(\boldsymbol{\omega})] \quad (4)$$

where $\alpha_i^{\text{IB}}(\boldsymbol{\omega})$ is the interband frequency-dependent polarizability of the i -th atom, and $\mathbf{E}_i^{\text{tot}}(\boldsymbol{\omega})$ is the total electric field acting on the i -th dipole, accounting for charge-dipole (\mathbf{E}^q), dipole-dipole (\mathbf{E}^μ), and dipole-field (\mathbf{E}^{ext}) interactions (see Ref. 16 for more details). For homogeneous materials, $\alpha_i^{\text{IB}}(\boldsymbol{\omega})$ is determined from the frequency-dependent bulk-permittivity, whereas in the case of multimetallic systems, the interband polarizability of the i -th atom is expressed as a function of the local composition of the system.^{16,17}

The ω FQF μ charge-dipole coupled equations can be recast in the following set of complex linear equations:

$$\begin{pmatrix} \mathbf{A}(\boldsymbol{\omega})\mathbf{T}^{\text{qq}} - \mathbf{Z}(\boldsymbol{\omega}) & \mathbf{A}(\boldsymbol{\omega})\mathbf{T}^{\text{q}\mu} \\ \mathbf{T}^{\mu\text{q}} & \mathbf{T}^{\mu\mu} - \mathbf{Z}^{\text{IB}}(\boldsymbol{\omega}) \end{pmatrix} \begin{pmatrix} \mathbf{q} \\ \boldsymbol{\mu} \end{pmatrix} = \begin{pmatrix} -\mathbf{A}(\boldsymbol{\omega})\mathbf{V}^{\text{ext}} \\ -\mathbf{E}^{\text{ext}} \end{pmatrix} \quad (5)$$

where $\mathbf{A}(\boldsymbol{\omega})$ is a frequency-dependent matrix containing NP chemical and geometrical parameters, while $\mathbf{Z}(\boldsymbol{\omega})$, and $\mathbf{Z}^{\text{IB}}(\boldsymbol{\omega})$ are diagonal matrices. \mathbf{T}^{qq} , $\mathbf{T}^{\text{q}\mu}$, $\mathbf{T}^{\mu\text{q}}$ and $\mathbf{T}^{\mu\mu}$ are charge-charge, charge-dipole, dipole-charge, and dipole-dipole interaction kernels, respectively (see Ref. 40 for more details).

When the linear system in Eq. 5 is solved, charges and dipoles modeling the optical intra- and interband response of the plasmonic NP are obtained. From such variables, the NP complex polarizability and the absorption cross-section $\sigma^{\text{abs}}(\boldsymbol{\omega})$ can be computed (See Ref. 16 and Ref. 17 for further details about the ω FQF μ model).

2.2 Solvent: the Fluctuating Charges model (FQ)

The physics governing the optical response of solvent systems is utterly different from that of plasmonic materials. When external electric fields are applied, solvent molecules might experience several phenomena ranging from electronic transitions to molecular rovibrations depending on the external field frequency. In the following, we focus only on solvents that are transparent in the spectral region where the plasmonic nanostructure absorbs light. Note that this is generally the case for noble metal nanoparticles, whose PRF falls within the visible range (400 - 700 nm).^{41,42} In this way, the external fields exciting the plasmons have energies lower than those of the electronic transitions of the solvent molecules but sufficiently high to quench rovibrational effects completely. Thus, the interaction with the external field only yields the polarization of the solvent's electron cloud. This is modeled by using the Fluctuating Charges (FQ) force field,¹⁸⁻²⁰ which has been extensively used in computational quantum chemistry for the modeling molecules in solution.^{21,23,43} Within FQ, each solvent atom is endowed with a charge \tilde{q} whose value is not fixed but can vary as a response to the external electric potential (see Fig. 1). Such charge fluctuation is governed by the electronegativity equalization principle (EEP),^{44,45} which states that at equilibrium, each atom has the same electronegativity, i.e. the negative of the chemical potential, as reported by Parr.⁴⁶ The FQ energy, i.e. the energy required to create a partial charge on each atom is generally written as a second-order Taylor expansion in the charges. For a polyatomic system, this can be written as:¹⁸

$$U(\tilde{\mathbf{q}}) = \sum_{\alpha,i} \left(\chi_{\alpha i} \tilde{q}_{\alpha i} + \frac{1}{2} \eta_{\alpha i} \tilde{q}_{\alpha i}^2 + \tilde{V}_{\alpha i}^{tot} \tilde{q}_{\alpha i} \right) + \sum_{\beta,k < \alpha,i} \tilde{q}_{\beta k} T_{\beta k, \alpha i}^{\tilde{q}\tilde{q}} \tilde{q}_{\alpha i} \quad (6)$$

where Greek and Roman indices run over molecules and atoms, respectively. $\chi_{\alpha i}$ is the electronegativity of the i -th atom of the α -th molecule, and $\mathbf{T}^{\tilde{q}\tilde{q}}$ is the charge-charge interaction kernel⁴⁰ of which the diagonal elements $\eta_{\alpha i}$ are chemical hardnesses, representing self-interaction polarization term. Both electronegativity and chemical hardness are well rooted in Conceptual Density Functional Theory⁴⁷ and are the only free parameters defining the model. Moreover, $\tilde{\mathbf{V}}^{tot}$ is the total external electric potential on each atomic site, which in the FQ case is the potential associated with the external optical field ($\tilde{\mathbf{V}}^{tot} = \tilde{\mathbf{V}}^{ext}$). To constrain the charge of each molecule Q_{α}^{tot} to a constant, a set of Lagrange multipliers λ_{α} is exploited. The energy

functional in Eq. 6 thus becomes:

$$F(\tilde{\mathbf{q}}, \boldsymbol{\lambda}) = U(\tilde{\mathbf{q}}) + \sum_{\alpha} \lambda_{\alpha} \left(\sum_i (\tilde{q}_{\alpha i}) - Q_{\alpha}^{tot} \right) \quad (7)$$

From the minimization of Eq. 7 with respect to the variables ($\tilde{\mathbf{q}}$ and $\boldsymbol{\lambda}$), the FQ polarization equations are obtained, implying that the electronic degrees of freedom of the solvent instantaneously rearrange without energy dissipation.¹⁸ Such an approximation is also valid for optical fields in the visible range and for transparent solvents.^{21,22,48} When the total electric field is monochromatic at frequency ω , the FQ polarization equations in the frequency domain read as follows (See Sec. S1.1 in the Supporting Information SI for further details):

$$\begin{pmatrix} \mathbf{T}^{\tilde{q}\tilde{q}} & \mathbf{1} \\ \mathbf{1}^t & \mathbf{0} \end{pmatrix} \begin{pmatrix} \tilde{\mathbf{q}}(\omega) \\ \boldsymbol{\lambda}(\omega) \end{pmatrix} = \begin{pmatrix} -\tilde{\mathbf{V}}^{ext}(\omega) \\ 0 \end{pmatrix} \quad (8)$$

where $\mathbf{1}$ is a rectangular matrix containing the blocks associated with the Lagrange multipliers. By solving Eq. 8, the atom-centered FQ charges, modeling the instantaneous polarization of the electronic cloud of the solvent under the application of an external monochromatic field, are obtained.

2.3 Optical response of a plasmonic nanoparticle in solution: the ω FQF μ /FQ model

ω FQF μ for describing the nanostructure's response and FQ for modeling solvent polarization are coupled in a multiscale fashion. In the resulting ω FQF μ /FQ approach, mutual polarization effects between the solvent and the metal NP are introduced (see Fig. 1). To this end, we include the solvent-induced electric potential $\mathbf{V}^{\tilde{q}}(\omega)$ and electric field $\mathbf{E}^{\tilde{q}}(\omega)$ acting on the NP's charges $\mathbf{q}(\omega)$ and dipoles $\boldsymbol{\mu}(\omega)$ respectively. Thus, the total chemical potential and field (Eq. 2 and Eq. 4 respectively) acting on each atomic site now read:

$$\phi_i(\omega) = V_i^q(\omega) + V_i^{\mu}(\omega) + V_i^{\tilde{q}}(\omega) + V_i^{ext}(\omega) \quad (9)$$

$$\mathbf{E}_i^{tot}(\omega) = \mathbf{E}_i^q(\omega) + \mathbf{E}_i^{\mu}(\omega) + \mathbf{E}_i^{\tilde{q}}(\omega) + \mathbf{E}_i^{ext}(\omega) \quad (10)$$

The electric potential and field induced by the FQ solvent charges $\tilde{\mathbf{q}}(\omega)$ on the NP's atomic sites read:

$$V_i^{\tilde{q}}(\omega) = \sum_{\alpha,k} T_{i,\alpha k}^{q\tilde{q}} \tilde{q}_{\alpha k}(\omega) \quad (11)$$

$$\mathbf{E}_i^{\tilde{q}}(\omega) = \sum_{\alpha,k} \mathbf{T}_{i,\alpha k}^{\mu\tilde{q}} \tilde{q}_{\alpha k}(\omega) \quad (12)$$

$\mathbf{T}^{q\tilde{q}}$ and $\mathbf{T}^{\mu\tilde{q}}$ are the Coulomb interaction kernels between the FQ solvent charges and ω FQF μ plasmonic charges and dipoles respectively, i.e.:

$$T_{ij}^{q\tilde{q}} = \frac{1}{|\mathbf{r}_{ij}|} \quad (13)$$

$$\mathbf{T}_{ij}^{\mu\tilde{q}} = \nabla_{r_i} T_{ij}^{q\tilde{q}} \quad (14)$$

where \mathbf{r}_{ij} is the distance between atoms i and j .

To account for mutual polarization effects, the total potential $\tilde{\mathbf{V}}^{\text{tot}}$ acting on the solvent atomic sites includes the potential generated by the NP's charges $\tilde{\mathbf{V}}^q(\omega)$ and dipoles $\tilde{\mathbf{V}}^\mu(\omega)$:

$$\tilde{V}_{\alpha i}^{\text{tot}}(\omega) = \tilde{V}_{\alpha i}^q(\omega) + \tilde{V}_{\alpha i}^\mu(\omega) \quad (15)$$

where the electric potential and field induced by the ω FQF μ charges and dipoles on the i -th solvent atom of the α -th molecule read:

$$\tilde{V}_{\alpha i}^q(\omega) = \sum_k T_{\alpha i,k}^{\tilde{q}q} q_k(\omega) \quad (16)$$

$$\tilde{V}_{\alpha i}^\mu(\omega) = \sum_k \mathbf{T}_{\alpha i,k}^{\tilde{q}\mu} \boldsymbol{\mu}_k(\omega) \quad (17)$$

Note that in Eq. 15 we neglect local field effects (i.e. $\tilde{V}_{\alpha i}^{\text{ext}}(\omega) = 0$).

The coupled ω FQF μ and FQ equations can thus be recast in a linear system defining the ω FQF μ /FQ

master equations:

$$\begin{pmatrix} \mathbf{A}(\omega)\mathbf{T}^{q\bar{q}} - \mathbf{Z}(\omega) & \mathbf{A}(\omega)\mathbf{T}^{q\mu} & \mathbf{A}(\omega)\mathbf{T}^{q\bar{q}} & \mathbf{0} \\ \mathbf{T}^{q\mu} & \mathbf{T}^{\mu\mu} - \mathbf{Z}^{\text{IB}}(\omega) & \mathbf{T}^{\mu\bar{q}} & \mathbf{0} \\ \mathbf{T}^{\bar{q}q,t} & \mathbf{T}^{\bar{q}\mu,t} & \mathbf{T}^{\bar{q}\bar{q}} & \mathbf{1} \\ \mathbf{0} & \mathbf{0} & \mathbf{1}^t & \mathbf{0} \end{pmatrix} \begin{pmatrix} \mathbf{q} \\ \mu \\ \bar{q} \\ \lambda \end{pmatrix} = \begin{pmatrix} -\mathbf{A}(\omega)\mathbf{V}^{\text{ext}}(\omega) \\ -\mathbf{E}^{\text{ext}}(\omega) \\ 0 \\ 0 \end{pmatrix} \quad (18)$$

By solving Eq.18, the charges and dipoles defining the response of the nanostructure as modified by the presence of the solvent are obtained. This allows the simulation of the optical response of plasmonic substrates with arbitrary shape and chemical composition embedded in a generic solvent or solvent mixture (See Sec. S1.2 in the SI).

3 Computational Protocol

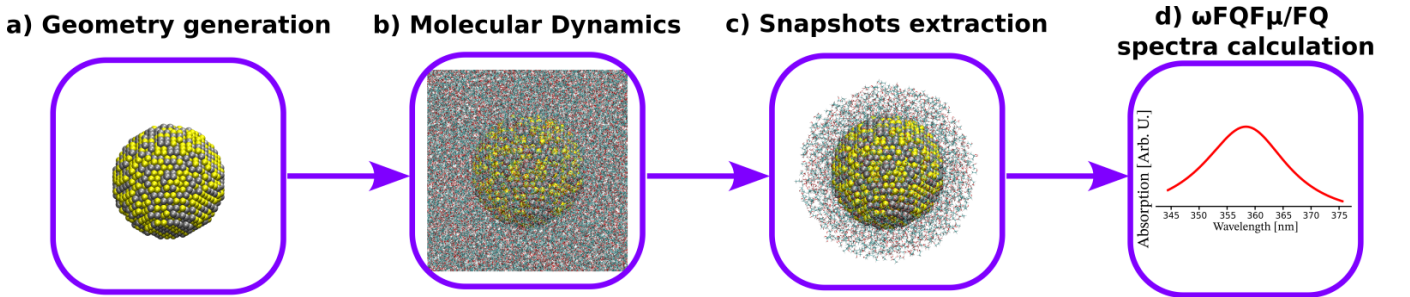


Figure 2: Graphical scheme of the computational protocol employed to compute $\omega\text{FQF}\mu/\text{FQ}$ absorption spectra of colloidal plasmonic NPs (see also Secs. S2.1-S2.4 in the SI).

In this work, we apply $\omega\text{FQF}\mu/\text{FQ}$ to the calculation of the absorption cross-section of plasmonic nanoparticles in solution. To reproduce the experimental PRF shift induced by solvent effects, the dynamic nature of the solvation phenomena needs to be properly described. To this end, we adapt the protocol designed for molecular systems in solution²¹ to the specific case of colloidal plasmonic NPs.

The protocol can be divided into four main steps (see Fig. 2):

- (i) *Geometry generation*: The geometry of isolated plasmonic NPs is generated by using an in-house code that employs the Atomic Simulation Environment (ASE) Python module v. 3.17⁴⁹ (see Fig. 2a and Sec. S2.1 in the SI)

- (ii) *Molecular Dynamics*: The nanostructure is solvated. To sample the NP-solvent phase-space, we perform a classical Molecular Dynamics (MD) simulation of the solvated colloidal system by using the GROMACS software package (version 2020.4) and a suitable force-field⁵⁰ (see Fig. 2b and Sec. S2.2 in the SI).
- (iii) *Extraction of structures*: From the MD trajectory, we extract 25 uncorrelated representative structures of the whole system. The number of structures ensures convergence of the spectral signal (see Sec. S2.4.2 in the SI). For each structure, we retain all solvent molecules that are at most 15 Å from the NP surface, resulting in a spherical droplet (see Fig. 2c) and Sec. S2.4.1 in the SI).
- (iv) *ω FQF μ /FQ spectral calculations*: For each spherical droplet, absorption cross sections are computed at the ω FQF μ /FQ level. The overall spectroscopic response is then recovered as the average over all structures (see Fig. 2d and Sec. S2.3 in the SI). All ω FQF μ /FQ calculations are performed by employing a stand-alone Fortran 95 package.

4 Results and Discussion

In this section, ω FQF μ /FQ is applied to compute the absorption properties of noble metal NPs in solution. First, the model is validated by reproducing reference data. Then, it is employed to study solvent effects on realistic homogeneous and bimetallic NPs dissolved in a pure solvent or a solvent mixture, showcasing the potential and flexibility of the approach.

4.1 Model Validation

The ω FQF μ /FQ approach is validated against vacuo-to-water PRF shifts of a small silver spherical-like cluster composed of 164 atoms (Ag_{164}). ω FQF μ /FQ values are compared to polarizable Time-Dependent Density Functional Tight Binding/Fluctuating Charges (TD-DFTB/FQ) calculations.³⁵ The advantageous computational scaling of TD-DFTB/FQ, which is reached through the approximation of two-electron interactions, makes it capable of handling larger systems than Time-Dependent Density Functional Theory-based methods (TD-DFT) while preserving accuracy.³⁵ The initial geometry of Ag_{164} is taken from Ref. 51: from

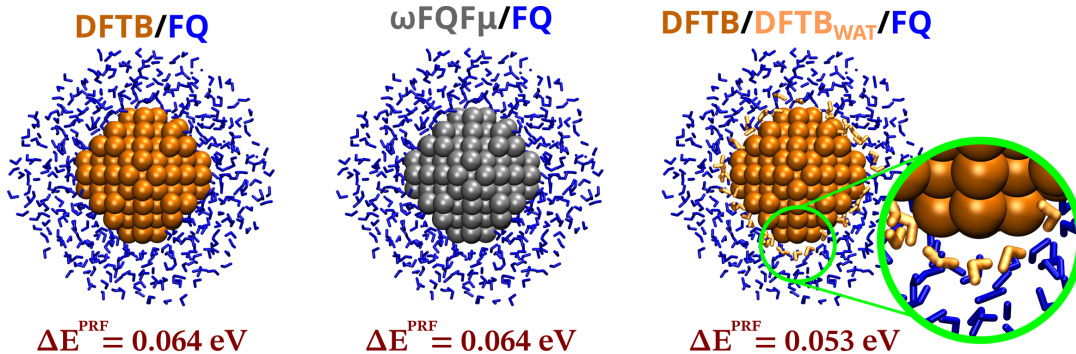


Figure 3: Vacuo-to-water PRF shifts (in eV) computed by using DFTB/FQ, ω FQF μ /FQ, and DFT/DFTB_{WAT}/FQ levels of theory. A graphical depiction of the structure used for each calculation is presented and the elements are colored according to the level of theory used (orange-DFTB, gray- ω FQF μ , blue-FQ). In the green inset a zoom of the DFTB/DFTB_{WAT}/FQ structure is reported to highlight the presence of water molecules treated at the DFTB level of theory (orange).

that structure, MD simulations in aqueous solution are run, a single random snapshot is extracted and cut in a spherical droplet containing water (WAT) molecules within 10 Å from the surface of the NP, resulting in a total number of 807 water molecules. Such distance is chosen to account for the most relevant NP-water interactions (See Sec. S2.4.1 in the SI). The absorption spectrum of Ag₁₆₄ in vacuo (i.e. by removing all water molecules from the snapshot) and in aqueous solution (Ag₁₆₄/WAT₈₀₇) are computed by using ω FQF μ and DFTB, and ω FQF μ /FQ and DFTB/FQ, respectively (see Sec. S2.5 in the SI for more details on the DFTB/FQ calculations). To evaluate quantum effects at the NP-solvent interface, we also performed DFTB/DFTB_{WAT}/FQ calculations, where the first solvation shell is treated at the DFTB level of theory (109 water molecules), whereas the remaining 698 WAT molecules are described at the FQ level. ω FQF μ parameters are recovered from Ref. 16. The FQ WAT molecules are modeled by using the parameters reported in Ref. 18 (WAT₁, see Tab. S1 in Sec. S2.3 in the SI). Note that additional calculations were performed by using the FQ parameters reported in Refs. 52–54 (see Sec. S3 in the SI).

In Fig. 3, we report the PRF shifts ($\Delta E^{\text{PRF}} = E^{\text{VAC}} - E^{\text{WAT}}$) in eV calculated at the DFTB/FQ level (panel A), ω FQF μ /FQ (panel B), and DFTB/DFTB_{WAT}/FQ (panel C).

All methods predict a very similar vacuo-to-water PRF redshift. The sign of the shift is expected due to the increase of the refractive index of the NP surrounding medium, as also supported by experimental observations.^{55,56} Notably, the hybrid DFTB/FQ and the fully classical ω FQF μ /FQ approaches predict the same solvatochromic shift (64 meV). This is particularly remarkable because the dimension of the studied

NP falls within the quantum size region, where quantum effects are expected to play a major role. Our results highlight the accuracy of $\omega\text{FQF}\mu$ in describing such structures.⁵⁷ When the first solvation shell of water molecules is described at the DFTB level (DFTB/DFTB_{WAT}/FQ), the predicted solvatochromic shift decreases by ~ 10 meV (53 meV). Such reduction can be attributed to the inclusion of purely quantum NP-solvent interactions, mainly related to Pauli repulsion effects,^{35,58,59} which are not taken into account by both DFTB/FQ and $\omega\text{FQF}\mu$ /FQ. Remarkably, the computational cost associated with $\omega\text{FQF}\mu$ /FQ is negligible as compared to DFTB-based methods (see Tab. S4 in the SI). Indeed, the favorable computational scaling of $\omega\text{FQF}\mu$ /FQ provides a substantial 99.4 % speed-up of the calculation with respect to DFTB/FQ, thus representing an effective, reliable, and cost-effective alternative to state-of-the-art *ab initio* methods.

4.2 Homogeneous colloidal NPs

The favorable computational scaling of $\omega\text{FQF}\mu$ /FQ opens up to computing the plasmonic response of large NPs in solution. We first consider homogeneous silver and gold spherical NPs (diameter = 5 nm, 3851 atoms) in aqueous solution, as modeled by using the WAT₁ parameterization.¹⁸ The average number of WAT molecules in the FQ region is 6464 (19392 atoms). Computed absorption cross-sections both in vacuo (VAC) and in water (WAT) are plotted in Fig. 4A-B, respectively, together with the corresponding vacuo-to-water PRF shifts ($\Delta\lambda$, in nm). The spectra of both systems are characterized by a main plasmonic band centered at about 360 nm (Ag NPs) and 570 nm (Au NPs). Au peaks are broader than Ag bands, in agreement with previous observations.^{60,61} In the studied region (300-800 nm), the spectra of Au systems are also characterized by the presence of a broad and intense band associated with interband absorption.¹⁶ When dissolved in solution, the main spectral features are maintained. However, we note that the plasmonic peak increases in intensity and slightly redshifts, in line with experimental data.^{9,55,56,62} For Ag, $\omega\text{FQF}\mu$ /FQ predicts a red-shift of the plasmonic peak larger than Au NPs, again in agreement with experiments.^{9,55,56,62} Such shift is due to the refractive index sensitivity (RIS) of the LSP, a quantity that is commonly exploited in plasmonic colorimetric sensors.^{29,30,63,64} RIS is generally expressed as $\Delta\lambda$ (in nm) over refractive index unit - $\Delta\lambda(\text{nm})/\text{RIU}$.

The computed $\omega\text{FQF}\mu$ /FQ RIS values are 15.0 nm/RIU for Ag and 7.9 nm/RIU for Au, while the experimentally measured RIS are 120-160 nm/RIU (Ag) and 70 nm/RIU (Au).^{29,30,63,64} Therefore, $\omega\text{FQF}\mu$ /FQ

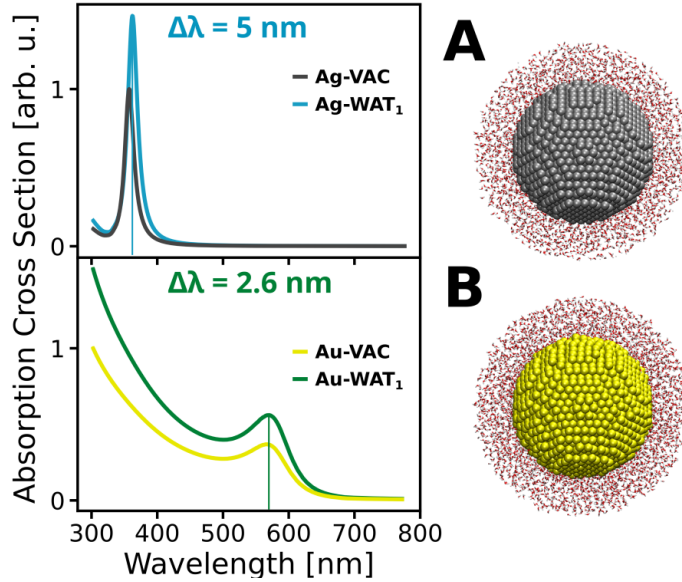


Figure 4: ω FQF μ /FQ absorption spectra of (A) Ag₃₈₅₁ and (B) Au₃₈₅₁ in vacuo (VAC) and water (WAT₁). $\Delta\lambda$ is the vacuo-to-water solvatochromic shift in nm. All spectra are normalized to the corresponding maximum in vacuo.

absolute RIS values are systematically lower than experimental ones for Ag and Au NPs, however ω FQF μ /FQ can nicely reproduce the experimental Ag/Au ratio (~ 2). The discrepancy can be related to the FQ parameters employed for modeling water, which have not been specifically tuned to describe solvated NPs.¹⁸ Nevertheless, although experimental absolute RIS values are underestimated by a factor of 10, the capability of ω FQF μ /FQ to match the Ag/Au sensitivity ratio is a remarkable feature of the model, which can be used to rationalize the optical behavior of plasmonic nanostructures with high RIS, with potential applications in sensor design.

4.3 Au@Ag core-shell colloidal NPs

By taking advantage of the favorable computational scaling of ω FQF μ /FQ, its atomistic nature, and its capability of correctly reproducing Ag/Au RI sensitivity ratio, the model is challenged to optimize the sensitivity of Au@Ag core-shell spherical NPs. In fact, colorimetric sensors exploiting the PRF shift of noble metals upon change of the local refractive index (RI) are widely used in biosensing.^{7,8,11,27–34} Among the various substrates used for this technology, gold-silver core-shell (Au@Ag) NPs are the most employed^{65–70} due to their high RIS.^{11,70} By studying such structures, we aim to showcase the potentialities of ω FQF μ /FQ, open up to colorimetric LSP sensor design.

We first consider spherical Au@Ag core-shell NPs (diameter = 5 nm, 3851 atoms) characterized by an Au core of increasing size ($d_{Au}=2, 3,$ and 4 nm – see Fig. 5A,B,C), in aqueous solution. To sample the NP-solvent phase space, we perform a classical MD simulation of a single Ag NP in the aqueous solution. We then construct the Ag@Au core-shell bimetallic NP by properly substituting the metal atoms after the MD snapshot’s extraction, which is a physically consistent procedure due to the almost equal lattice constants of the two metals.⁷¹ On average, 6464 water molecules are considered in the FQ region and modeled employing the WAT₁ parameterization.¹⁸

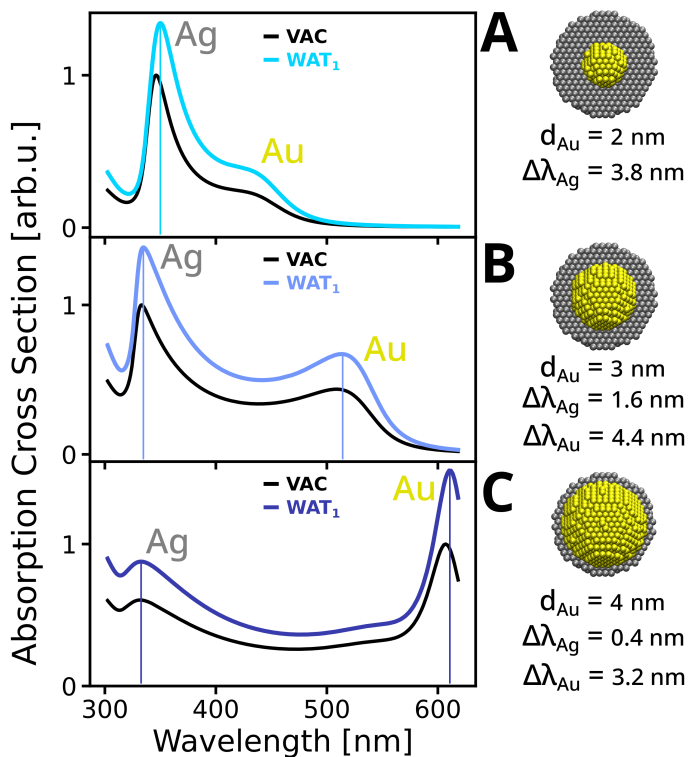


Figure 5: ω FQF μ /FQ absorption spectra of core-shell Au@Ag spherical NPs in vacuo (VAC) and in aqueous solution (WAT₁) as a function of the diameter of the Au core (d_{Au} : (A) 2.0 nm, (B) 3.0 nm and (C) 4.0 nm). The solvatochromic shifts of “Ag” ($\Delta\lambda_{Ag}$) and “Au” ($\Delta\lambda_{Au}$) peaks are reported in nm. All spectra are normalized to the maximum in vacuo.

In Fig. 5, ω FQF μ /FQ absorption spectra of Au@Ag core-shell NPs in vacuo (black) and water (blue) are reported. For all structures, absorption spectra in vacuo and solution feature two main bands at short (~ 350 nm) and long wavelengths (> 400 nm), in agreement with previous theoretical and experimental observations.^{11,12,72,73} Such peaks are located in the spectral region of the plasmon bands of pure Ag and Au spheres (see Fig. 4A,B). For this reason, we call them “Ag” and “Au” peaks, respectively. Their position and

intensity strongly depend on the diameter of the Au core both in the gas phase and solution. In particular, by first focusing on vacuo results, for Au-core thickness of 1 nm (Fig. 5A), the “Ag” peak, located around 346 nm, dominates the computed spectrum, while the “Au” band appears as a shoulder. By increasing the Au-core size, the “Ag” peak slightly blueshifts of about 10 nm while decreasing in intensity. On the contrary, the “Au” peak largely redshifts of about 150 nm, and significantly increases in intensity, becoming dominant for Au-core diameters of 4 nm (1 nm Ag-shell thickness). Including the solvent redshifts both “Ag” and “Au” peaks and increases their intensity. The shift differs for each peak and each Au-core diameter. In particular, all “Ag” peaks show lower solvatochromic shifts as compared to pure Ag spheres ($\Delta\lambda = 5.0$ nm see Fig. 4A), and increasing the Au-core size reduces the redshift of the “Ag” peak from $\Delta\lambda_{Ag} = 3.8$ nm ($d_{Au} = 2$ nm) to $\Delta\lambda_{Ag} = 0.4$ nm ($d_{Au} = 4$ nm). The shift of the “Au” peak is generally larger (e.g. $\Delta\lambda_{Au} = 4.4$ nm for $d_{Au} = 2$ nm) than that of a pure Au sphere ($\Delta\lambda = 2.6$ nm, see Fig. 4B). This suggests that for small NPs ($d \sim 5$ nm), the “Au” peak RIS can be increased by coating the NP with an Ag layer. Remarkably, our findings align with previous theoretical and experimental observations.^{11,67,70}

To showcase more potentialities of ω FQF μ /FQ, we now move to study the effect of alloying the Ag shell on the refractive index sensitivity, for which an atomistic picture is essential.¹⁷ Note that, to the best of our knowledge, the use of atomistic modeling in this field has received only a little attention.^{11,12,74}

We consider a substantially more complex system composed of a spherical Au@Ag core-shell bimetallic NP (see Fig. 6) of 5 nm of diameter (3851 atoms) with an Au core of diameter (d_{Au}) of 3 nm, and featuring a 50% Ag 50%Au random bimetallic layer of 1 nm. Such NP is solvated in aqueous solution, exploiting the same procedure discussed above. Fig. 6, shows computed ω FQF μ /FQ absorption cross-section (σ^{abs}) both in vacuo and water. The computed spectrum substantially deviates from the corresponding perfect core-shell system (Fig. 5B). In fact, the “Au” peak is shifted at higher wavelengths (~ 600 nm) and dominates the spectrum, while the “Ag” peak disappears in a dim spectral feature between 350 nm and 500 nm. Remarkably, the computed PRF shift of the gold peak ($\Delta\lambda_{Au}$) is 8.4 nm, almost double the original Au@Ag core-shell structure ($\Delta\lambda_{Au} = 4.4$ nm, see Fig. 5B), and more than three times than a pure Au sphere of the same dimensions ($\Delta\lambda = 2.6$ nm, see Fig. 4). Remarkably, the same trend is also obtained for the computed ω FQF μ /FQ RIS sensitivity, which reaches 25.5 nm/RIU. The obtained results thus suggest that the alloying of the Ag shell of an Au@Ag core shell can potentially improve the refractive index sensitivity of the system

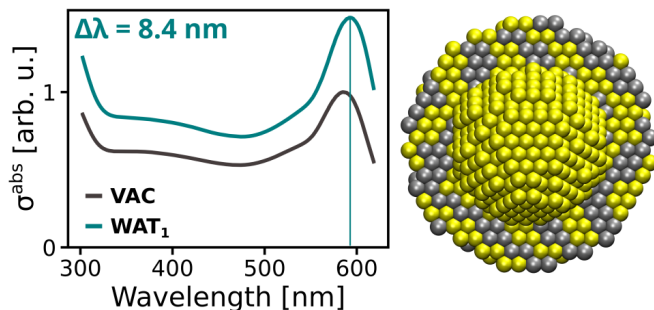


Figure 6: ω FQF μ /FQ absorption cross section (σ^{abs}) of core-shell Au@Ag spherical NP with an Au core diameter of 3 nm and featuring an alloyed (50% Au/Ag) external layer of 1 nm (see right panel) in vacuo (VAC) and aqueous solution (WAT₁). $\Delta\lambda$ indicates the solvatochromic shift (in nm). All spectra are normalized to the maximum in vacuo.

by almost a factor of 2.

To finally showcase the flexibility of ω FQF μ /FQ, we solvate the NP in a 1:1 water-ethanol mixture (WAT-ETH). The even more complex chemical nature of this system enforces the need for a fully atomistic model to simulate its optical properties. To the best of our knowledge, ω FQF μ /FQ is the first fully atomistic model capable of calculating the response of a generic multimetallic plasmonic NP embedded in a multicomponent solvent.

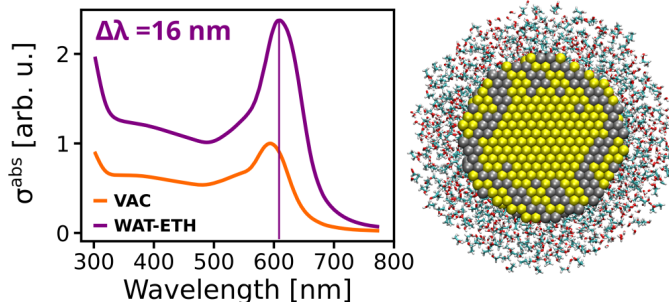


Figure 7: ω FQF μ /FQ absorption cross section (σ^{abs}) of core-shell Au@Ag spherical NP with an Au core diameter of 3 nm and featuring an alloyed (50% Au/Ag) external layer of 1 nm (see right panel) in vacuo (VAC) and a 1:1 water-ethanol mixture (WAT-ETH). The vacuo-to-mixture solvatochromic shift is given in nm. All spectra are normalized to the maximum in vacuo.

To sample the NP-solvent phase space, we perform a classical MD simulation of a single Ag NP in the WAT-ETH mixture. We then construct the Ag@Au core-shell bimetallic NP by properly substituting the metal atoms after the MD snapshot extraction. The FQ parameterization employed for the water molecules is WAT₁, while for ethanol we exploit the parameters proposed in Ref. 54 (see Tab.S1 in the SI). On average

1800 ETH and 1218 WAT molecules are included in the spherically-shaped snapshot (i.e. 19854 atoms in total).

In Fig. 7, the absorption spectrum of the complex bimetallic Au/Ag NP both in vacuo (VAC) and solvated in the 1:1 water-ethanol mixture (WAT-ETH) is graphically depicted, together with the corresponding computed PRF shift ($\Delta\lambda$ in nm). Notably, absorption spectra both in vacuo and in solution present a sharp peak around 600 nm which can be assigned to the Au plasmonic dipolar band, and a shoulder at about 350-400 nm associated with the Ag plasmonic absorption. Solvent effects provided by the WAT-ETH mixture lead to a huge enhancement of the peak absorption (almost twice that in vacuo), which is also red-shifted by 16 nm. Considering a refractive index for the WAT-ETH mixture of 1.36,⁷⁵ a computed RIS of about 44.0 nm/RIU is obtained. Such a value is almost twice that obtained in pure water, highlighting a non-trivial RIS dependence on the solvent composition.

5 Summary and Conclusions

We have presented a novel fully atomistic multiscale classical model, named ω FQF μ /FQ, which is capable of simulating the optical properties of real-size plasmonic colloidal nanoparticles (NPs) of a generic chemical nature. ω FQF μ /FQ is a multiscale model based on the mutual electrostatic interaction between the solvent and the NP. More specifically, the interaction of the plasmonic substrate with the external optical field is modeled employing ω FQF μ ,^{16,17} where each atom is endowed with a frequency-dependent charge and dipole, modeling intraband and interband plasmon decaying mechanisms, respectively. The solvent environment is considered transparent to the optical radiation and its instantaneous polarization is modeled through the polarizable FQ force field.¹⁸⁻²⁰

ω FQF μ /FQ has been challenged to reproduce reference TD-DFTB/FQ values, showing an almost perfect match with the TD-DFTB/FQ vacuo-to-water plasmon resonance frequency (PRF) shift of a small silver cluster (Ag₁₆₄), with a substantial 99.4 % speed-up of the calculation. Then, we have showcased the capabilities of ω FQF μ /FQ by simulating the optical properties of real-size homogeneous Ag and Au spherical NPs (\sim 5 nm of diameter, 3851 metal atoms with 6464 water molecules), highlighting how the computed ratio between the refractive index sensitivities of Au and Ag NPs matches the experiments. Remarkably,

$\omega\text{FQF}\mu/\text{FQ}$ can also be used to study the sensitivity of colorimetric LSP sensors, as demonstrated by the chemical substitution of Au atoms in Au@Ag core-shell NPs, which can potentially enhance the sensitivity by a factor $2 \sim 3$. Finally, the flexibility of $\omega\text{FQF}\mu/\text{FQ}$ is validated by simulating the absorption spectrum of a bimetallic Ag/Au NP solvated in a 1:1 water-ethanol mixture. Remarkably, the model can be applied to any solvent or solvent mixtures, including green solvents,⁷⁶ pending a reliable parametrization of the FQ force field.⁵⁴

In conclusion, $\omega\text{FQF}\mu/\text{FQ}$ is the first fully atomistic classical model capable of providing a platform for the calculation of LSP shifts of plasmonic NPs with the accuracy of *ab-initio* methodologies for systems in the quantum confinement size region, but with a computational cost that consents its application to realistic-sized colloidal NPs. Such a development can potentially pave the way for future in-silico rational design of colorimetric sensors.

Acknowledgments

We gratefully acknowledge the Center for High-Performance Computing (CHPC) at SNS for providing the computational infrastructure.

Supporting Information

Details on $\omega\text{FQF}\mu/\text{FQ}$, computational details, convergence of $\omega\text{FQF}\mu/\text{FQ}$ spectra as a function of the radius of the solvent droplet and number of snapshots, MD analysis for spherical NPs (diameter = 5 nm) in solution.

References

- (1) Mayer, K. M.; Hafner, J. H. Localized surface plasmon resonance sensors. *Chem. Rev.* **2011**, *111*, 3828–3857.
- (2) McNamara, K.; Tofail, S. A. Nanoparticles in biomedical applications. *Adv. Phys. X* **2017**, *2*, 54–88.

- (3) Dutta, A.; Medda, A.; Patra, A. Recent advances and perspectives on colloidal semiconductor nanoplatelets for optoelectronic applications. *J. Phys. Chem. C* **2020**, *125*, 20–30.
- (4) Hu, X.; Li, G.; Yu, J. C. Design, fabrication, and modification of nanostructured semiconductor materials for environmental and energy applications. *Langmuir* **2010**, *26*, 3031–3039.
- (5) Yang, P.; Zheng, J.; Xu, Y.; Zhang, Q.; Jiang, L. Colloidal synthesis and applications of plasmonic metal nanoparticles. *Adv. Mater.* **2016**, *28*, 10508–10517.
- (6) Chen, H.; Shao, L.; Woo, K. C.; Ming, T.; Lin, H.-Q.; Wang, J. Shape-dependent refractive index sensitivities of gold nanocrystals with the same plasmon resonance wavelength. *J. Phys. Chem. C* **2009**, *113*, 17691–17697.
- (7) Lee, J.-H.; Kim, B.-C.; Oh, B.-K.; Choi, J.-W. Highly sensitive localized surface plasmon resonance immunosensor for label-free detection of HIV-1. *Nanomedicine* **2013**, *9*, 1018–1026.
- (8) Kim, J.; Oh, S. Y.; Shukla, S.; Hong, S. B.; Heo, N. S.; Bajpai, V. K.; Chun, H. S.; Jo, C.-H.; Choi, B. G.; Huh, Y. S., et al. Heteroassembled gold nanoparticles with sandwich-immunoassay LSPR chip format for rapid and sensitive detection of hepatitis B virus surface antigen (HBsAg). *Biosens. Bioelectron.* **2018**, *107*, 118–122.
- (9) Chen, H.; Kou, X.; Yang, Z.; Ni, W.; Wang, J. Shape-and size-dependent refractive index sensitivity of gold nanoparticles. *Langmuir* **2008**, *24*, 5233–5237.
- (10) Foerster, B.; Joplin, A.; Kaefer, K.; Celiksoy, S.; Link, S.; Sönnichsen, C. Chemical interface damping depends on electrons reaching the surface. *ACS nano* **2017**, *11*, 2886–2893.
- (11) Steinbrück, A.; Stranik, O.; Csaki, A.; Fritzsche, W. Sensoric potential of gold–silver core–shell nanoparticles. *Anal. Bioanal. Chem.* **2011**, *401*, 1241–1249.
- (12) Szántó, G.; Csarnovics, I.; Bonyár, A. Numerical investigation of the refractive index sensitivity of Au/Ag core-shell nanostructures for sensing applications. *Sens. Bio-Sens. Res.* **2021**, *32*, 100414.
- (13) Hu, Y.; Zhang, A.-Q.; Li, H.-J.; Qian, D.-J.; Chen, M. Synthesis, study, and discrete dipole approximation simulation of Ag-Au bimetallic nanostructures. *Nanoscale Res. Lett.* **2016**, *11*, 1–9.

- (14) Hsiao, A.; Gartia, M. R.; Chang, T.-W.; Wang, X.; Khumwan, P.; Liu, G. L. Colorimetric plasmon resonance microfluidics on nanohole array sensors. *Sens. Bio-Sens. Res.* **2015**, *5*, 24–32.
- (15) Yamada, A. Computational Analyses of Plasmonics of a Silver Nanoparticle in a Vacuum and in a Water Solution by Classical Electronic and Molecular Dynamics Simulations. *J. Phys. Chem. A* **2022**, *126*, 4762–4771.
- (16) Giovannini, T.; Bonatti, L.; Lafiosca, P.; Nicoli, L.; Castagnola, M.; Illobre, P. G.; Corni, S.; Cappelli, C. Do We Really Need Quantum Mechanics to Describe Plasmonic Properties of Metal Nanostructures? *ACS Photonics* **2022**,
- (17) Nicoli, L.; Lafiosca, P.; Grobas Illobre, P.; Bonatti, L.; Giovannini, T.; Cappelli, C. Fully atomistic modeling of plasmonic bimetallic nanoparticles: nanoalloys and core-shell systems. *Front. Photon.* **2023**, *4*, 1199598.
- (18) Rick, S. W.; Stuart, S. J.; Berne, B. J. Dynamical fluctuating charge force fields: Application to liquid water. *J. Chem. Phys.* **1994**, *101*, 6141–6156.
- (19) Rick, S. W.; Stuart, S. J.; Bader, J. S.; Berne, B. Fluctuating charge force fields for aqueous solutions. *J. Mol. Liq.* **1995**, *65*, 31–40.
- (20) Rick, S. W.; Berne, B. Dynamical fluctuating charge force fields: the aqueous solvation of amides. *J. Am. Chem. Soc.* **1996**, *118*, 672–679.
- (21) Giovannini, T.; Egidi, F.; Cappelli, C. Molecular spectroscopy of aqueous solutions: a theoretical perspective. *Chem. Soc. Rev.* **2020**, *49*, 5664–5677.
- (22) Giovannini, T.; Egidi, F.; Cappelli, C. Theory and algorithms for chiroptical properties and spectroscopies of aqueous systems. *Phys. Chem. Chem. Phys.* **2020**, *22*, 22864–22879.
- (23) Gómez, S.; Giovannini, T.; Cappelli, C. Multiple facets of modeling electronic absorption spectra of systems in solution. *ACS Physical Chemistry Au* **2023**, *3*, 1–16.
- (24) Giovannini, T.; Cappelli, C. Continuum vs. atomistic approaches to computational spectroscopy of solvated systems. *Chem. Commun.* **2023**, *59*, 5644–5660.

- (25) Mennucci, B.; Corni, S. Multiscale modelling of photoinduced processes in composite systems. *Nat. Rev. Chem.* **2019**, *3*, 315–330.
- (26) Xia, Y.; Halas, N. J. Shape-controlled synthesis and surface plasmonic properties of metallic nanostructures. *MRS Bull.* **2005**, *30*, 338–348.
- (27) Loiseau, A.; Zhang, L.; Hu, D.; Salmain, M.; Mazouzi, Y.; Flack, R.; Liedberg, B.; Boujday, S. Core–shell gold/silver nanoparticles for localized surface plasmon resonance-based naked-eye toxin biosensing. *ACS Appl. Mater. Interfaces* **2019**, *11*, 46462–46471.
- (28) Piliarik, M.; Šířpová, H.; Kvasnička, P.; Galler, N.; Krenn, J. R.; Homola, J. High-resolution biosensor based on localized surface plasmons. *Opt. Express* **2012**, *20*, 672–680.
- (29) Mock, J. J.; Smith, D. R.; Schultz, S. Local refractive index dependence of plasmon resonance spectra from individual nanoparticles. *Nano lett.* **2003**, *3*, 485–491.
- (30) Underwood, S.; Mulvaney, P. Effect of the solution refractive index on the color of gold colloids. *Langmuir* **1994**, *10*, 3427–3430.
- (31) Rycenga, M.; Cobley, C. M.; Zeng, J.; Li, W.; Moran, C. H.; Zhang, Q.; Qin, D.; Xia, Y. Controlling the synthesis and assembly of silver nanostructures for plasmonic applications. *Chem. Rev.* **2011**, *111*, 3669–3712.
- (32) Haes, A. J.; Van Duyne, R. P. A unified view of propagating and localized surface plasmon resonance biosensors. *Anal. Bioanal. Chem.* **2004**, *379*, 920–930.
- (33) Anker, J. N.; Hall, W. P.; Lyandres, O.; Shah, N. C.; Zhao, J.; Van Duyne, R. P. Biosensing with plasmonic nanosensors. *Nat. Mater* **2008**, *7*, 442–453.
- (34) Stewart, M. E.; Anderton, C. R.; Thompson, L. B.; Maria, J.; Gray, S. K.; Rogers, J. A.; Nuzzo, R. G. Nanostructured plasmonic sensors. *Chem. Rev.* **2008**, *108*, 494–521.
- (35) Lafiosca, P.; Gómez, S.; Giovannini, T.; Cappelli, C. Absorption properties of large complex molecular systems: the DFTB/fluctuating charge approach. *J. Chem. Theory Comput.* **2022**, *18*, 1765–1779.

- (36) Giovannini, T.; Rosa, M.; Corni, S.; Cappelli, C. A classical picture of subnanometer junctions: an atomistic Drude approach to nanoplasmonics. *Nanoscale* **2019**, *11*, 6004–6015.
- (37) Giovannini, T.; Bonatti, L.; Polini, M.; Cappelli, C. Graphene plasmonics: Fully atomistic approach for realistic structures. *J. Phys. Chem. Lett.* **2020**, *11*, 7595–7602.
- (38) Bonatti, L.; Nicoli, L.; Giovannini, T.; Cappelli, C. In silico design of graphene plasmonic hot-spots. *Nanoscale Adv.* **2022**, *4*, 2294–2302.
- (39) Maier, S. A., et al. *Plasmonics: fundamentals and applications*; Springer, 2007; Vol. 1.
- (40) Giovannini, T.; Puglisi, A.; Ambrosetti, M.; Cappelli, C. Polarizable QM/MM approach with fluctuating charges and fluctuating dipoles: the QM/FQF μ model. *J. Chem. Theory Comput.* **2019**, *15*, 2233–2245.
- (41) Litjens, R. A.; Quickenden, T. I.; Freeman, C. G. Visible and near-ultraviolet absorption spectrum of liquid water. *Appl. Opt.* **1999**, *38*, 1216–1223.
- (42) Sani, E.; Dell’Oro, A. Spectral optical constants of ethanol and isopropanol from ultraviolet to far infrared. *Opt. Mater.* **2016**, *60*, 137–141.
- (43) Nicoli, L.; Giovannini, T.; Cappelli, C. Assessing the quality of QM/MM approaches to describe vacuo-to-water solvatochromic shifts. *J. Chem. Phys.* **2022**, *157*.
- (44) Mortier, W. J.; Van Genechten, K.; Gasteiger, J. Electronegativity equalization: application and parametrization. *J. Am. Chem. Soc.* **1985**, *107*, 829–835.
- (45) Sanderson, R. An interpretation of bond lengths and a classification of bonds. *Science* **1951**, *114*, 670–672.
- (46) Parr, R. G. Density functional theory. *Annu. Rev. Phys. Chem.* **1983**, *34*, 631–656.
- (47) Geerlings, P.; De Proft, F.; Langenaeker, W. Conceptual density functional theory. *Chem. Rev.* **2003**, *103*, 1793–1874.
- (48) Cappelli, C. Integrated QM/polarizable MM/continuum approaches to model chiroptical properties of strongly interacting solute–solvent systems. *Int. J. Quantum Chem.* **2016**, *116*, 1532–1542.

- (49) Larsen, A. H. et al. The atomic simulation environment—a Python library for working with atoms. *J. Phys.: Condens. Matter* **2017**, *29*, 273002.
- (50) Abraham, M. J.; Murtola, T.; Schulz, R.; Páll, S.; Smith, J. C.; Hess, B.; Lindahl, E. GROMACS: High performance molecular simulations through multi-level parallelism from laptops to supercomputers. *SoftwareX* **2015**, *1*, 19–25.
- (51) Liu, Z.; Alkan, F.; Aikens, C. M. TD-DFTB study of optical properties of silver nanoparticle homodimers and heterodimers. *J. Chem. Phys.* **2020**, *153*.
- (52) Carnimeo, I.; Cappelli, C.; Barone, V. Analytical gradients for MP 2, double hybrid functionals, and TD-DFT with polarizable embedding described by fluctuating charges. *J. Comput. Chem.* **2015**, *36*, 2271–2290.
- (53) Giovannini, T.; Lafiosca, P.; Chandramouli, B.; Barone, V.; Cappelli, C. Effective yet reliable computation of hyperfine coupling constants in solution by a QM/MM approach: Interplay between electrostatics and non-electrostatic effects. *J. Chem. Phys.* **2019**, *150*, 124102.
- (54) Ambrosetti, M.; Skoko, S.; Giovannini, T.; Cappelli, C. Quantum mechanics/fluctuating charge protocol to compute solvatochromic shifts. *Journal of Chemical Theory and Computation* **2021**, *17*, 7146–7156.
- (55) Zhang, C.; Sun, L.-D.; Yan, C.-H. Noble metal plasmonic nanostructure related chromisms. *Inorganic Chemistry Frontiers* **2016**, *3*, 203–217.
- (56) Lee, Y. H.; Chen, H.; Xu, Q.-H.; Wang, J. Refractive index sensitivities of noble metal nanocrystals: the effects of multipolar plasmon resonances and the metal type. *J. Phys. Chem. C* **2011**, *115*, 7997–8004.
- (57) Liebsch, A. Surface-plasmon dispersion and size dependence of Mie resonance: silver versus simple metals. *Phys. Rev. B* **1993**, *48*, 11317.
- (58) Giovannini, T.; Ambrosetti, M.; Cappelli, C. Quantum confinement effects on solvatochromic shifts of molecular solutes. *J. Phys. Chem. Lett.* **2019**, *10*, 5823–5829.
- (59) Amovilli, C.; Floris, F. M. On the effect of solute-solvent Pauli repulsion on $n \rightarrow \pi^*$ transition for acrolein in water solution. *Phys. Chem. Liq.* **2020**, *58*, 281–289.

- (60) Hottin, J.; Wijaya, E.; Hay, L.; Maricot, S.; Bouazaoui, M.; Vilcot, J.-P. Comparison of gold and silver/gold bimetallic surface for highly sensitive near-infrared SPR sensor at 1550 nm. *Plasmonics* **2013**, *8*, 619–624.
- (61) Dengler, S.; Kübel, C.; Schwenke, A.; Ritt, G.; Eberle, B. Near-and off-resonant optical limiting properties of gold–silver alloy nanoparticles for intense nanosecond laser pulses. *J. Opt.* **2012**, *14*, 075203.
- (62) Ghosh, S. K.; Nath, S.; Kundu, S.; Esumi, K.; Pal, T. Solvent and ligand effects on the localized surface plasmon resonance (LSPR) of gold colloids. *J. Phys. Chem. B* **2004**, *108*, 13963–13971.
- (63) Malinsky, M. D.; Kelly, K. L.; Schatz, G. C.; Van Duyne, R. P. Chain length dependence and sensing capabilities of the localized surface plasmon resonance of silver nanoparticles chemically modified with alkanethiol self-assembled monolayers. *J. Am. Chem. Soc.* **2001**, *123*, 1471–1482.
- (64) Nath, N.; Chilkoti, A. Label free colorimetric biosensing using nanoparticles. *J. Fluoresc.* **2004**, *14*, 377–389.
- (65) Mao, K.; Yang, Z.; Li, J.; Zhou, X.; Li, X.; Hu, J. A novel colorimetric biosensor based on non-aggregated Au@ Ag core–shell nanoparticles for methamphetamine and cocaine detection. *Talanta* **2017**, *175*, 338–346.
- (66) Dong, P.; Wu, Y.; Guo, W.; Di, J. Plasmonic biosensor based on triangular Au/Ag and Au/Ag/Au core/shell nanoprisms onto indium tin oxide glass. *Plasmonics* **2013**, *8*, 1577–1583.
- (67) Sun, L.; Li, Q.; Tang, W.; Di, J.; Wu, Y. The use of gold-silver core-shell nanorods self-assembled on a glass substrate can substantially improve the performance of plasmonic affinity biosensors. *Microchim. Acta* **2014**, *181*, 1991–1997.
- (68) Hao, J.; Xiong, B.; Cheng, X.; He, Y.; Yeung, E. S. High-throughput sulfide sensing with colorimetric analysis of single Au–Ag core–shell nanoparticles. *Anal. Chem.* **2014**, *86*, 4663–4667.
- (69) Guo, Y.; Wu, J.; Li, J.; Ju, H. A plasmonic colorimetric strategy for biosensing through enzyme guided growth of silver nanoparticles on gold nanostars. *Biosens. Bioelectron.* **2016**, *78*, 267–273.

- (70) Fu, Q.; Zhang, D.; Yi, M.; Wang, X.; Chen, Y.; Wang, P.; Ming, H. Effect of shell thickness on a Au–Ag core–shell nanorods-based plasmonic nano-sensor. *J. Opt.* **2012**, *14*, 085001.
- (71) Haynes, W. *CRC Handbook of Chemistry and Physics*; CRC Press: Boca Raton, 2014.
- (72) Chen, Y.; Wu, H.; Li, Z.; Wang, P.; Yang, L.; Fang, Y. The study of surface plasmon in Au/Ag core/shell compound nanoparticles. *Plasmonics* **2012**, *7*, 509–513.
- (73) Peña-Rodríguez, O.; Pal, U. Au@ Ag core–shell nanoparticles: efficient all-plasmonic Fano-resonance generators. *Nanoscale* **2011**, *3*, 3609–3612.
- (74) Ma, Y.-W.; Zhang, L.-H.; Wu, Z.-W.; Yi, M.-F.; Zhang, J.; Jian, G.-S. The study of tunable local surface plasmon resonances on Au-Ag and Ag-Au core-shell alloy nanostructure particles with DDA method. *Plasmonics* **2015**, *10*, 1791–1800.
- (75) Oelke, W.; Arnold, R. The Refractive Indices of Alcohol-Water Mixture at 25° C. Proceedings of the Iowa Academy of Science. 1936; pp 175–176.
- (76) Atilhan, M.; Aparicio, S. Molecular dynamics simulations of metal nanoparticles in deep eutectic solvents. *J. Phys. Chem. C* **2018**, *122*, 18029–18039.